



저작자표시-비영리 2.0 대한민국

이용자는 아래의 조건을 따르는 경우에 한하여 자유롭게

- 이 저작물을 복제, 배포, 전송, 전시, 공연 및 방송할 수 있습니다.
- 이차적 저작물을 작성할 수 있습니다.

다음과 같은 조건을 따라야 합니다:



저작자표시. 귀하는 원저작자를 표시하여야 합니다.



비영리. 귀하는 이 저작물을 영리 목적으로 이용할 수 없습니다.

- 귀하는, 이 저작물의 재이용이나 배포의 경우, 이 저작물에 적용된 이용허락조건을 명확하게 나타내어야 합니다.
- 저작권자로부터 별도의 허가를 받으면 이러한 조건들은 적용되지 않습니다.

저작권법에 따른 이용자의 권리는 위의 내용에 의하여 영향을 받지 않습니다.

이것은 [이용허락규약\(Legal Code\)](#)을 이해하기 쉽게 요약한 것입니다.

[Disclaimer](#) 

공학석사 학위논문

**Comparison of Two Computational
Models to Estimate Gold Nanoparticle
Radio-enhancement**

금나노입자의 방사선 증감 효과를 예측하는
두 가지 전산 모델 비교

2021년 02월

서울대학교 융합과학기술대학원

융합과학부 방사선융합의생명전공

김혜진

Comparison of Two Computational Models to Estimate Gold Nanoparticle Radio-enhancement

지도 교수 예성준

이 논문을 공학석사 학위논문으로 제출함

2021년 02월



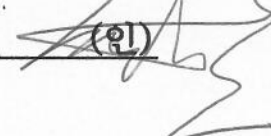
서울대학교 융합과학기술대학원

융합과학부 방사선융합의생명전공

김혜진

김혜진의 공학석사 학위논문을 인준함

2021년 02월

위원장	이강원	(인) 
부위원장	예성준	(인) 
위원	성원모	(인) 

ABSTRACT

Comparison of Two Computational Models to Estimate Gold Nanoparticle Radio-enhancement

Hyejin Kim

Program in Biomedical Radiation Sciences

Department of Transdisciplinary Studies

Graduate School of Convergence Science and Technology

Seoul National University

Numerous experiments have strongly supported the application of gold nanoparticles (GNPs) as radio-enhanced agents. In the previous study, the local effect model (LEM I) was developed to predict the cell survival for MDA-MB-231 cells exposed to 150 kVp x-rays after 500 $\mu\text{g/ml}$ GNPs treatment. However, measurable microdosimetric quantities could not be obtained, which were correlated with biological effects on cells. Thus, a microdosimetric kinetic model (MKM) was applied for GNP radio-enhancement (GNP-MKM), which uses the microdosimetric quantities such as dose-mean lineal energy. Using the Monte Carlo simulation tool Geant4, the dose-mean lineal energy with secondary radiations from GNPs and the radial dose distributions around a GNP were estimated. The variations in MKM parameters for different photon energies, domain sizes, and GNP concentrations were calculated to compare the survival fractions predicted by

both models. As a result of GNP-MKM, the domain size of 500 nm represented pairwise combinations of DSBs making it hard to repair the DNA damage. It contributes to the idea that the DNA repair mechanisms have been modified, which make the biological effect of the intracellular GNPs as radiosensitizers in addition to radioenhancers. With a domain radius of 500 nm and a threshold dose of 20 Gy, the sensitizer enhancement ratio (SER) predicted by GNP-MKM and GNP-LEM was 1.41 and 1.29, respectively. The GNP-MKM predictions much strongly depended on the domain size than GNP-LEM did on the threshold dose. It is able to provide another method to predict survival fraction for the GNP radio-enhancement.

Keywords: Gold Nanoparticle, Radio-enhancement, Microdosimetric-Kinetic Model, Local Effect Model, Survival Fraction, Monte Carlo Simulation

Student Number: 2017-27243

List of Tables

Table 1. Summary of LEM and MKM.....	7
Table 2. An example of calculation method for frequency mean lineal energy from Geant4 simulation. Among the parameters in the Table, y range is an example to show how to draw the lineal energy frequency graph. Lineal energy for i -th event belongs to the $(k-1)$ -th bin of lineal energy histogram.	16
Table 3. The interaction probability per Gy at 1 mm depth between 1.9nm single GNP and different photon sources	22
Table 4. Dose-mean lineal energy, \bar{y}_D with different domain sizes, r_d of secondary radiations from GNP incident with 150 kVp x-ray.....	25
Table 5. Comparison of GNP-MKM MKM ($r_d = 500 \text{ nm}$) and GNP-LEM ($D_t = 20 \text{ Gy}$) by using a simple cell geometry irradiated by 150 kVp x-ray with different GNP concentrations.....	32
Table 6. Comparison of GNP-MKM MKM ($r_d = 500 \text{ nm}$) and GNP-LEM ($D_t = 20 \text{ Gy}$) by using real cell geometry obtained from five ODT images irradiated by 150 kVp x-ray with 500 $\mu\text{m}/\text{ml}$ GNPs	33

List of Figures

- Figure 1. Domain size and biological effects of radiation; Lethal lesions are produced either by simple chromosome breaks or by pairwise combination of Double Strand Breaks (DSBs), leading to a 2-Break Aberration (2-BA). The spatial scales associated with each case are of the order of nanometers and micrometers, respectively (Modified from [17]). 3
- Figure 2. Modeling geometry of cell (yellow) and nucleus (green) with (a) no GNP and (b) various GNP concentrations (1×10^6 , 5×10^6 , 1×10^7 , 5×10^7 #/cell)..... 10
- Figure 3. Schematic diagrams of reprocessing ODT image to get GNP distributions and nucleus geometry: (a) The voxels with RI > 1.38 were considered as a cluster of GNPs. Each selected voxel is assumed to contain a constant GNP concentration measured by ICP-MS (b) The cell nucleus was manually segmented and reconstructed as a polygon..... 11
- Figure 4. Principle of lineal energy scoring for a single incident beam. The Geant4 ($i-1$)th event illustrated in this figure contains 10 energy depositions. The scoring sphere is placed at a random distance which is less or equal to the domain radius (light blue circle). It is in a random direction from a randomly selected energy deposition (red circle). In this illustration, the lineal energy is obtained by summing the three energy depositions contained in the domain sphere, and its associated statistical weight is taken as 10/3..... 15
- Figure 5. An example of lineal energy frequency, $f(y)$ corresponding to **Table 2**. Weighting w_i is added according to which range the lineal energy generated in the i -th event belongs. Finally, $f(y)$ is the summation of all weightings in each bin. 17
- Figure 6. Schematic diagram for \bar{y}_D simulation geometry (not to scale) (a) The phase space file (phsp1) was recorded for 150 kVp x-ray photon beam passing a 1.9 cm

diameter area at 1 mm depth in a macroscopic water phantom. (b) A 1.9 nm GNP was irradiated by the phsp1 in vacuum. The outgoing electrons were scored in a phase space file (phsp2) on the surface of GNP. (c) The phase space was used as a point source at each center of GNPs of which positions were based on ODT images. (d) The domain volume is randomly placed within the nucleus and one energy deposition was sampled to produce lineal energy (y). 19

Figure 7. Validation of microdosimetric spectra (a) Frequency-mean lineal energy and (b) dose-mean lineal energy as a function of incident electron kinetic energy, in scoring spheres of 500 nm radius; Black circles: “option 2” constructor (default models); green squares: “option 4” constructor (Ioannina models); pink triangles: “option 6” constructor (CPA100 models); Reproduced from [32] for validation. 24

Figure 8. (a) Frequency weighted lineal energy spectra (b) dose weighted lineal energy spectra of 500 nm domain radius; the bin width of the x-axis is set as 0.05. 26

Figure 9. Cell nucleus reconstructed from ODT images: (a) Cell nucleus polygon displayed in 3D program (b) Image-based cell nucleus and GNP distributions imported to the Geant4 simulation tool..... 28

Figure 10. Average refractive index values for various regions in a cell which is treated by 1.9 nm GNPs of 500 $\mu\text{m}/\text{ml}$ for 24 hours. 29

Figure 11. Integrated gold signal of ODT images from 5 cells for increasing distance from the nuclear membrane. The gold intensity reduces significantly across the membrane (distance = 0) and the gold signal within the nucleus (distance < 0) is consistent with the assumption that all of the gold is nearly outside the nuclear membrane. 30

Figure 12. Experimentally observed cell survival for MDA-MB-231 cells exposed to 1, 3, and 6 Gy of 150 kVp x-rays (red square = with GNP; blue diamond = without GNP) and theoretically predicted survival fraction with GNPs (black triangle by LEM; yellow circle by MKM). Error bars are one standard deviation at each corresponding dose-survival fraction point. 34

Figure 13. SER sensitivity of adjustable parameters in the models expressed as a percentage of SER changes with $\pm 25\%$ and $\pm 50\%$ of D_t (=20 Gy) and r_d (=500 nm)..... 35

CONTENTS

ABSTRACT	i
List of Tables	iii
List of Figures	iv
1. Introduction	1
2. Material and Methods	4
2.A. Principle of GNP-LEM	4
2.B. Principle of GNP-MKM	5
2.C. Clonogenic assay and GNP uptakes	8
2.D. Cellular geometry and GNP distributions	9
2.E. MC simulation of D_n	12
2.F. MC simulation of y_D	14
2.G. Comparison of GNP-LEM and GNP-MKM	20
3. Results	21
3.A. Common variables in both models	21
3.B. MC simulation of y_D	23
3.C. Cellular geometry and GNP distributions	27
3.D. Comparison of GNP-MKM and GNP-LEM	31
4. Discussion	36
5. Conclusions	39
REFERENCES	40
Abstract (in Korean)	46

1. Introduction

The radiotherapy purpose is to maximize cancer cell death, while minimizing the damage to healthy tissue. In radiation therapy, advances over the past twenty years have been largely driven by the use of intensity-modulated radiation therapy (IMRT) and volume-modulated radiation therapy (VMAT), along with other technological advances. It has been shown that the introduction of gold nanoparticles (GNPs) into cancer cells enhances the radiative effects in the cells, further improving their therapeutic potential. Especially, in the past decade, interest in the use of GNPs as radiation sensitizers has dramatically increased [1]. This interest was initially driven by their biocompatibility, easy surface modifications and, a high photoelectric interaction probability. When GNPs are targeted to cancer cells, auger- and photo- electrons are generated by a kilovoltage photon beam and deposit their energies at the μm level, effectively killing only cancer cells without affecting surrounding normal cells. Hainfeld et al. [2] has firstly observed a decrease in tumor size when injecting GNPs into rat blood vessels and irradiating kV radiation. Subsequent studies have further demonstrated the effect of GNP radio-enhancement on investigated animals and cells [3-6].

However, observed radio-enhancement is often much greater than the predictions by simple macroscopic dose models [1]. It is suggested that the microscopic dose enhancement should be considered to predict cell survival with GNPs. The GNP-mediated radiation has the characteristics of accumulating energy deposition in microscopic local areas [7-11], similar to dose profiles in hadron treatments such as carbon beams. Therefore, the local effective model (LEM) and the microdosimetric-kinetic model (MKM) are good candidates for calculating the increased biological effectiveness with GNPs. The LEM is used clinically for treatment planning at the Heidelberg Ion-beam therapy center, Germany and the MKM is used at the Heavy Ion Medical Accelerator of NIRS in Chiba, Japan.

Previous studies have successfully predicted the survival fraction by applying the

original version of LEM (LEM I) to GNP mediated radio-enhancement (GNP-LEM) [10, 12-14]. Compare to LEM I, the extended model takes into account in more detail the clusters of damage by using damage enhancement factor [15]. The GNP-LEM revealed the importance of GNP distribution and cell geometry [14]. Recently developed GNP-LEM using real cell geometry and gold distribution has shown good agreement with experimental survival fraction [13]. Although it provides the macroscopic endpoint of biological cell survival, the microdosimetric quantities have never been obtained.

Instead, MKM estimates the survival curves from a dose-mean lineal energy (\bar{y}_D), which is defined as one of microdosimetric quantities in ICRU36 [16]. These quantities are important because they can, in principle, be measured and correlated with biological effects [17]. \bar{y}_D is adjustable to “domain,” which is a critical target volume in the cell nucleus. For example, the lethal lesions are produced either by simple chromosome breaks or by pairwise combination of Double Strand Breaks (DSBs), leading to a 2-Break Aberration (2-BA). The domain sizes associated with each case are of the order of nanometers and micrometers, respectively (**Figure 1**). However, it has rarely been tried to apply MKM to estimate GNP-mediated cell survival fraction. Hsing group [18] calculated GNP radio-enhancement in the ratio of dose-mean lineal energies with and without gold by using a gold-coated plugged TEPC. Although the measured radio-enhancement of 1.3 is within the range of data from in vitro observations, GNP concentration is not considered in the study. And they considered the relative values to be relative biological effect (RBE). However, the original MKM uses absolute dose-mean lineal energy with linear quadratic (LQ) equation.

In this study, full GNP-MKM was developed to calculate the GNP radio-enhancement at a local point, which depends on GNP concentrations. To compare the results from GNP-LEM, the same optical diffraction tomography (ODT) cell images from the previous study [13] were used. The crucial parameters of GNP-LEM and GNP-MKM were compared. The parameter sensitivities on sensitizer enhancement ratio (SER) were also investigated.

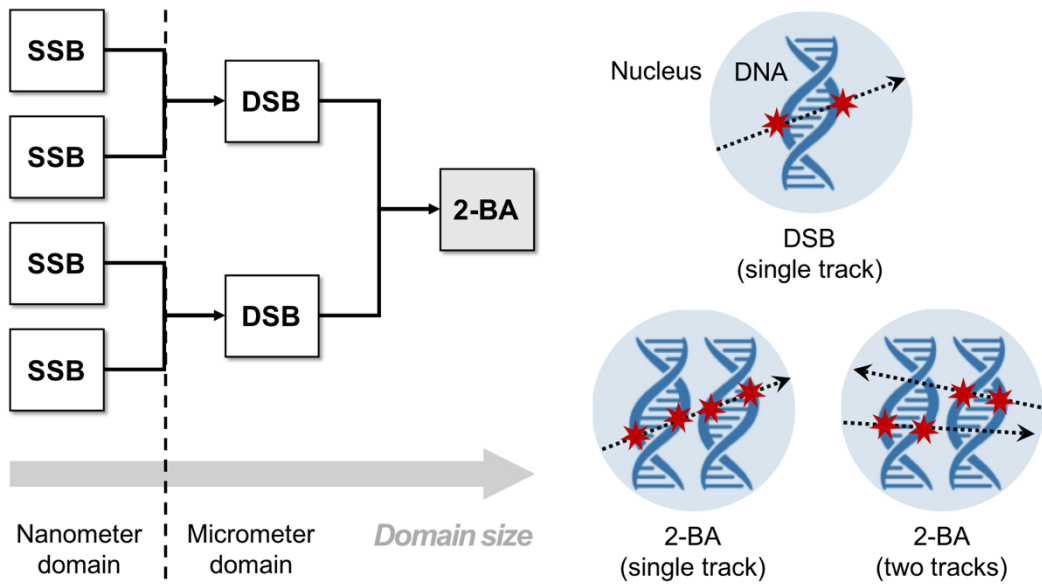


Figure 1. Domain size and biological effects of radiation; Lethal lesions are produced either by simple chromosome breaks or by pairwise combination of Double Strand Breaks (DSBs), leading to a 2-Break Aberration (2-BA). The spatial scales associated with each case are of the order of nanometers and micrometers, respectively (Modified from [17]).

2. Material and Methods

2.A. Principle of GNP-LEM

The basic assumption of the LEM is that equal local doses on a subcellular scale lead to equal local damages, independent of the energy and type of radiation [14]. It assumes that the cell nucleus is the principal target with a similar concept to MKM. Within the LEM framework, the number of lethal events in the nucleus (L_n) follows a Poisson distribution as a function of absorbed dose in infinitesimally small volume in the nucleus (d). Therefore, the surviving fraction (S) as a function of photon dose is determined by

$$S = \exp(-\langle L_n(d) \rangle) \quad (1)$$

$$L_n(d) = \begin{cases} \alpha d + \beta d^2 & (d \leq D_t) \\ (\alpha + 2\beta D_t)d - \beta D_t^2 & (d > D_t) \end{cases} \quad (2)$$

$$d = D(1 + p \cdot d_{GNP}) \quad (3)$$

where descriptions of the terms are given in **Table 1**. Note that since it is practically difficult to precisely determine the photon dose response curve at very high doses, the most critical parameter is the threshold dose (D_t) among those parameters. D_t is usually kept as an adjustable parameter in order to allow the best representation of the experimental data.

The ‘GNP-LEM’, three inputs were needed: 1) the linear quadratic model to parameterize the reference x-ray dose response curve into α and β components, 2) a spatial dose distribution around a GNP for a given particle source, and 3) a geometrical model of the cell to characterize the volume of the nucleus and the distribution of the GNPs [12]. The first parameter was taken from clonogenic assay. To obtain the second parameter, the radial dose per ionization of single GNP and the interaction probability per Gray (p)

were required. For the third parameters, two types of geometrical cellular models were considered. One was a simple cell geometry to investigate the model's dependency on different GNP concentrations. The other was the 3D live cell geometry from optical diffraction tomography (ODT) images. The amount of GNP uptake was estimated using inductively coupled plasma-mass spectroscopy (ICP-MS).

2.B. Principle of GNP-MKM

The most significant difference between the MKM and the LEM is related to the definition of the input parameters. The basic assumption of MKM is that the principal target is the cell nucleus, which is divided into virtual spheres of radius (r_d), referred to as "domains." [19] It is hypothesized that the local dose effect of each domain is related to a survival fraction for x-rays. The summation of the local effect in all domains determines the survival probability with GNPs. Unlike the LEM, the MKM estimates the increased local dose effect from dose-mean lineal energy (\bar{y}_D), which is measured with a spherical proportional counter or calculated by Monte Carlo simulation [19-22]. Within the MKM framework, the number of lethal events in the nucleus (L_n) follows a Poisson distribution as a function of dose. Thus, the surviving fraction as a function of photon dose is determined by

$$S = \exp(-\langle L_n(D_n) \rangle) \quad (4)$$

$$\langle L_n(D_n) \rangle = \alpha^* D_n + \beta D_n^2 \quad (5)$$

$$\alpha^* = \alpha + \beta \frac{\bar{y}_D}{\rho \pi r_d^2} \quad (6)$$

where descriptions of the terms are given in **Table 1**. Among those parameters, the domain size (r_d) is an adjustable variable to adjust the number of lethal events in combination with

the photon survival curve.

The ‘GNP-MKM’, three inputs were needed: 1) the linear quadratic model to parameterize the reference x-ray dose response curve into α and β components, 2) absorbed dose in the nucleus (D_n), and 3) the microdosimetric quantities (\bar{y}_D and r_d). The first parameter was taken from clonogenic assay which is a common variable with GNP-LEM. To obtain the second parameter, the radial dose per ionization of single GNP (d_{GNP}) and the interaction probability per Gray (p) were required with a concept similar to GNP-LEM. The third parameters were calculated by MC simulation described in the next section. Note that in the GNP-MKM, α^* was newly calculated as shown in equation (6). It was assumed that the former term in the right-hand side of equation (6) is due to the reference x-ray and the latter term is related to the secondary radiations resulted from gold and photon interactions. Therefore, only secondary radiations from GNPs were considered when calculating dose-mean lineal energy (\bar{y}_D).

Table 1. Summary of LEM and MKM

	LEM I	MKM
Similarities [19]	a) The cell nucleus is the principal target. b) It is divided into small independent domains. c) A survival fraction for X-rays is adopted as the local dose effect of each domain. d) The summation of the local effect in all domains determines the survival probability.	
Domain size [19]	Infinitesimally small volume (a purely theoretical model)	Subcellular volume (simulated or estimated by using mini-TEPC)
Adjustable Parameter [16, 19]	Threshold dose (D_t)	Domain radius (r_d)
Formulas [10, 20-23]	$L_n(d) = \begin{cases} \alpha d + \beta d^2 & (d \leq D_t) \\ (\alpha + 2\beta D_t)d - \beta D_t^2 & (d > D_t) \end{cases}$ $S = \exp(-\langle L_n(d) \rangle)$	$L_n(D) = \alpha^* D + \beta D^2$ $= \left(\alpha + \beta \frac{\bar{y}_D}{\rho \pi r_d^2} \right) D + \beta D^2$ $S = \exp(-\langle L_n(D) \rangle)$
Application to GNP radio- enhancement [12-14]	$L_n(d) = \begin{cases} \alpha d + \beta d^2 & (d \leq D_t) \\ (\alpha + 2\beta D_t)d - \beta D_t^2 & (d > D_t) \end{cases}$ $d = D(1 + p \cdot d_{GNP})$ $S = \exp(-\langle L_n(d) \rangle)$	$\langle L_n(D_n) \rangle = \alpha^* D_n + \beta D_n^2$ $= \left(\alpha + \beta \frac{\bar{y}_D}{\rho \pi r_d^2} \right) D_n + \beta D_n^2$ $D_n = \frac{\sum_{i=1}^N D(1 + p \cdot (d_{GNP})_i)}{N}$ $S = \exp(-\langle L_n(D_n) \rangle)$
Glossary	d Absorbed dose in infinitesimally small volume in the nucleus [Gy] D_n Average absorbed dose in the nucleus [Gy] α Coefficient of D in relation between $\ln S$ and D for reference radiation [Gy^{-1}] α^* Coefficient of D in relation between $\ln S$ and D calculated by MKM [Gy^{-1}] β Coefficient of D^2 in relation between $\ln S$ and D for reference radiation [Gy^{-2}] ρ Density of a domain (=1 g/ml) \bar{y}_D Dose-mean lineal energy [keV/ μm] p Interaction probability per Gray [Gy^{-1}] L_n Number of lethal lesions in infinitesimally small volume in the nucleus i Number of subvolumes in the nucleus (=1~ N) D Prescribed dose (macroscopically average dose to a population of cells) [Gy] d_{GNP} Total radial dose per ionization from all GNPs in infinitesimally small volume in the nucleus [Gy] r_d Radius of a domain [nm] S Surviving fraction D_t Threshold dose [Gy] $(d_{GNP})_i$ Total radial dose per ionization from all GNPs deposited at i -th subvolume [Gy]	

2.C. Clonogenic assay and GNP uptakes

The clonogenic assay allows assessment of the cytotoxicity of radiation by testing the ability of a single cell to grow into a colony, i.e. to undergo continuous proliferation. The cell is considered radio-biologically dead if it has lost its reproductive viability to produce progeny [24]. This type of assay has developed into the most extensively used technique for evaluating the radiation sensitivity of different cell lines and it is considered the “gold standard” for radiation response. Conventionally, the outcomes of colony formation assays are presented as so-called survival curves representing the survival fraction, i.e. the number of colonies that are formed after treatment, as a function of radiation dose. The plating efficiency is calculated by

$$PE = \frac{\text{Number of colonies formed}}{\text{Number of cells seeded}} \times 100 \text{ [\%]} \quad (7)$$

$$S = \frac{\text{Number of colonies formed after treatment}}{\text{Number of cells seeded} \times PE} \quad (8)$$

where S is the fraction of surviving cells.

In this study, it was performed for cells exposed to the 500 $\mu\text{g/ml}$ of 1.9 nm GNPs (Nanoprobes Inc., Yaphank, NY). They were incubated for 24h, irradiated and incubated for 2 weeks. The resulting cell colonies were stained and counted. Survival fractions were then calculated relative to non-treated cells.

The GNP uptake assessment was also prepared with the same conditions as above and performed using inductively coupled plasma-mass spectrometry (ICP-MS). Using the mass spectrometer, the gold ions were separated by their mass-to-charge ratio. Then, a detector received a signal proportional to the gold concentration in the sample. The gold content was determined using PerkinElmer[®] SCIEX NexION[®] 350D (Shelton, CT), which has a low detection limit at the parts per billion (ppb) range.

2.D. Cellular geometry and GNP distributions

Two types of geometrical cellular models were considered to characterize the volume of the nucleus and the distribution of the GNPs. A simple cell geometry was used to investigate the model's dependency on different GNP concentrations. The cell diameter was decided as 13.5 μm with an 8 μm diameter nucleus at the center (**Figure 1**), which is in good agreement with the range of many cancer cell lines [25]. From transmission electron microscopy (TEM) and fluorescence images of MDA-MB-231 cells treated with 1.9 nm GNPs, it is confirmed that their distribution is mainly around the nucleus [4, 25-27] (**Figure 1. (b)**).

Using a commercial ODT (HT-1H; Tomocube Inc., Daejeon, Korea), three dimensional intracellular localization of GNPs inside the cells was quantified using their high refractive index (RI) values. Cells were plated for 24h and exposed to GNPs for another 24h for ODT imaging. Image reconstruction was performed using commercial software (Tomostudio; Tomocube Inc., Daejeon, Korea). The voxel size of the tomograms obtained by this system was $0.098 \times 0.098 \times 0.195 \mu\text{m}^3$. These 3D images were then imported into an in-house software program in MATLAB[®] version 2016b (MathWorks[®] Inc., Natick, MA) for image segmentation. The intracellular localization of GNPs was assumed to be in the regions where the refractive index (RI) values were higher than those of the normal cytoplasm (>1.38) [13, 28] (**Figure 2. (a)**). In the range of RI values higher than 1.38, a larger number of counts was observed in the GNP-treated cells compared to the control cells. In addition, it has been reported that the RI values of the cell cytoplasm is in the range of 1.37 to 1.39. Large amounts of aggregated GNPs were internalized into the cell, i.e., in cytoplasmic lysosomes and these aggregated GNPs were dispersed in the cytoplasm. Each selected voxel is assumed to contain a constant GNP concentration measured by ICP-MS [13]. The cell nucleus was manually segmented [29] and reconstructed as a polygon (**Figure 2. (b)**).

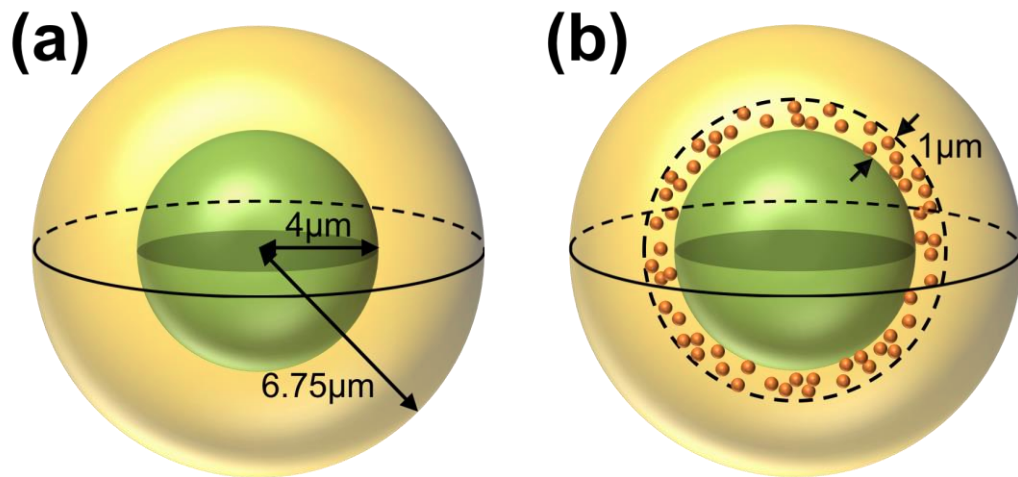


Figure 2. Modeling geometry of cell (yellow) and nucleus (green) with (a) no GNP and (b) various GNP concentrations (1×10^6 , 5×10^6 , 1×10^7 , 5×10^7 #/cell)

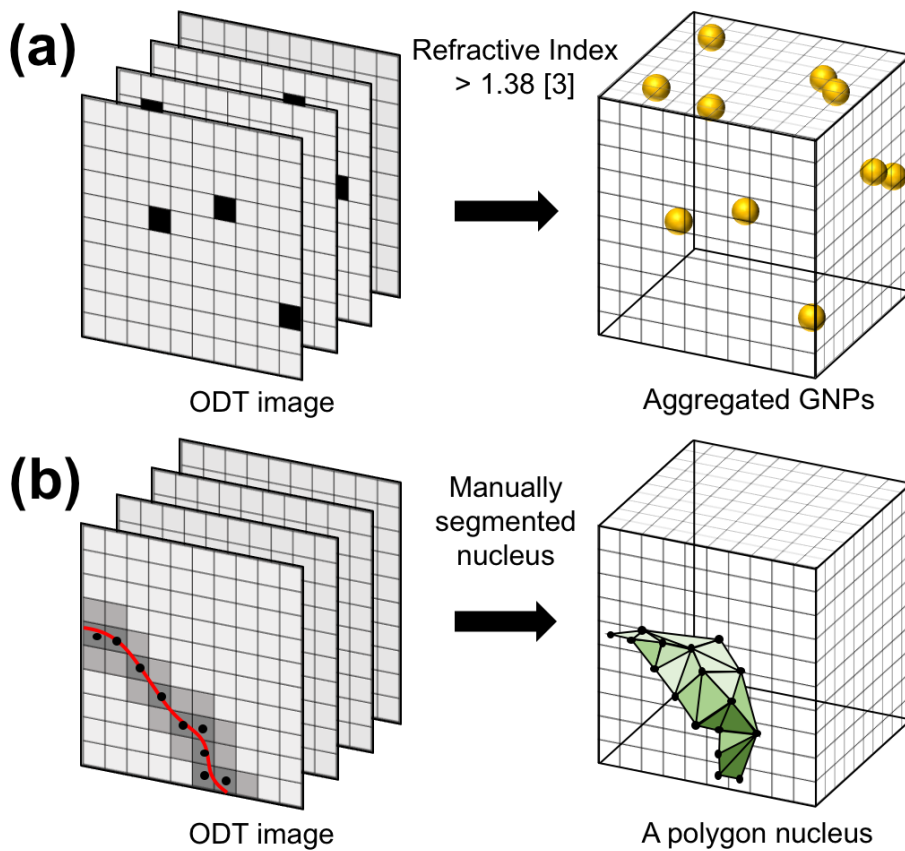


Figure 3. Schematic diagrams of reprocessing ODT image to get GNP distributions and nucleus geometry: (a) The voxels with RI > 1.38 were considered as a cluster of GNPs. Each selected voxel is assumed to contain a constant GNP concentration measured by ICP-MS (b) The cell nucleus was manually segmented and reconstructed as a polygon

2.E. MC simulation of D_n

Monte Carlo simulations were performed to calculate the interaction probability (p) using Geant4 simulation toolkit (version. Geant4.10.5) [30, 31]. The toolkit has the advantage of adding an electromagnetic physics model to describe particle matter interactions in the low energy range, especially below the MeV range [32]. The Geant4 low energy electromagnetic Penelope physics model was used. The range cut for all particles was set to 1 nm and electrons were tracked down to 100 eV. The standard Geant4-DNA default physics list [33-35] was used to track electrons in water. Atomic de-excitation processes, including fluorescence, auger electron emission and Auger cascades, were activated in all the below simulations.

To get an absorbed dose in the nucleus (D_n), the radial dose of a single ionizing event by single GNP (d_{GNP}) and the interaction probability per Gray (p) were calculated. To investigate the dependency of p on beam types, the three photon sources were investigated: 1) a 150 kVp polychromatic x-ray beam (with a 2 mm aluminum filter) acquired by SpekCalc 1.1 [36], 2) a 6MV FFF source originated from Tillikainen et al. [37], and 3) a ^{192}Ir radionuclide photon spectrum isotope [38]. The phase space files were acquired at 1 mm depth in water phantom to reflect the experimental condition. The total interaction probability was determined by the probability that a random photon in the phase space file passes through a GNP and a probability of photon interacting with a GNP [14]. The size of phase space file was change from the scored phase space file in the water phantom to the microscopic phase space used to irradiate the GNP. Note that each particle was weighted by $1/\cos(\theta)$ based on the angle (θ) between its original direction and the beam axis to account for contributions of laterally scattered electrons. Thus, the interaction probability per dose (p) can be calculated as,

$$p = \left(\frac{R_{GNP}}{R_{phsp}} \right)^2 \times N_{track} \quad (9)$$

where R_{GNP} , R_{phsp} , and N_{track} are the radius of the GNP, the radius of the phase space acquired in a macroscopic water phantom, and the number of particle tracks that causes an ionization in the GNP volume for incoming particles depositing 1 Gy in a water phantom. The photon contribution of the particle spectrum was evaluated by filtering the incoming particle beam to contain only electrons. To confirm the radio-enhancement, the simulations were repeated, replacing GNPs with water nanoparticles (WNPs) under the same conditions. In case of p , the photon contribution of the particle spectrum was evaluated by filtering the incoming particle beam to contain only electrons. The radial dose from single GNP was calculated in spherical shells of 10 nm thickness around the source [13].

Assuming the nucleus is divided into N subvolumes, additional dose due to GNPs at i -th subvolume ($i = 1 \sim N$) was determined by multiplying the dose of a single ionizing event by all GNPs at i -th subvolume ($(d_{GNP})_i$), the interaction probability per Gray (p), and the prescribed dose (D). Then, average absorbed dose in nucleus was calculated by

$$D_n = \frac{\sum_{i=1}^N D(1 + p \cdot (d_{GNP})_i)}{N} \quad (10)$$

2.F. MC simulation of \bar{y}_D

The dose-mean lineal energy (\bar{y}_D) was calculated by using Geant4 simulation toolkit (version. Geant4.10.5) [30, 31]. The default domain radius (r_d) was set to be 500 nm. The domain volume was randomly placed within the nucleus and one energy deposition was sampled to produce lineal energy (y) [32]. It is defined as $y = \epsilon/\bar{l}$, where ϵ is the energy deposited in the domain by one event and \bar{l} is the mean chord length of the domain [16].

$$yd(y) = \frac{y^2 f(y)}{\int_0^\infty y f(y) dy} = \frac{y^2 f(y)}{\bar{y}_F} \quad (11)$$

$$\bar{y}_F = \int_0^\infty y f(y) dy \quad (12)$$

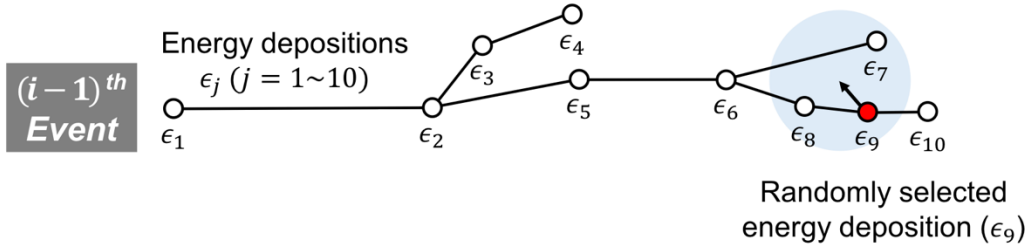
Here $d(y) = yf(y)/\bar{y}_F$ is introduced as the dose probability density of lineal energy. $f(y)$ is usually characterized by the frequency mean lineal energy, \bar{y}_F . The dose-mean lineal energy (\bar{y}_D) is calculated [16] as

$$\bar{y}_D = \int_0^\infty y d(y) dy = \frac{\int_0^\infty y^2 f(y) dy}{\int_0^\infty y f(y) dy} = \frac{\int_0^\infty y^2 f(y) dy}{\bar{y}_F} \quad (13)$$

Especially for Geant4 simulation, detailed calculation steps were illustrated in **Figure 4**. The scoring sphere is placed at a random distance which is less or equal to the domain radius [32]. It is in a random direction from a randomly selected energy deposition. For example, in ($i-1$)-th event, the lineal energy is obtained by summing the three energy depositions contained in the domain sphere, and its associated statistical weight is taken as 10/3 (**Figure 4**). **Table 2** shows an example of calculation method for frequency mean lineal energy. Among the parameters in the Table, y range is an example to show how to draw the lineal energy frequency graph in **Figure 5**. Lineal energy for i -th event belongs to the ($k-1$)-th bin of lineal energy histogram.

Random direction and placement of domain sphere center; associated weight (w_{i-1}) is 10/3

$$y_{i-1} = \sum_{j=7..9} \epsilon_j / \bar{l}$$



Random direction and placement of domain sphere center; associated weight (w_i) is 9/2

$$y_i = \sum_{j=3,4} \epsilon_j / \bar{l}$$

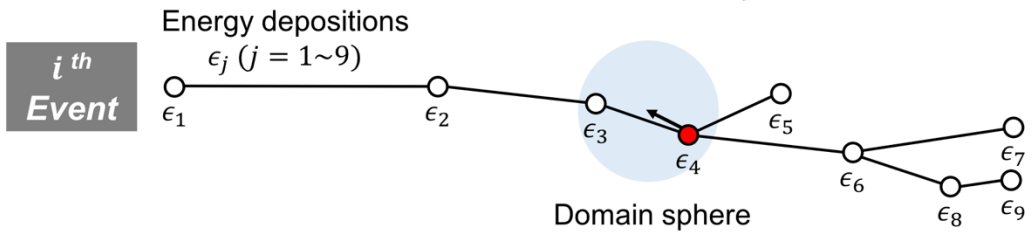


Figure 4. Principle of lineal energy scoring for a single incident beam. The Geant4 $(i-1)^{th}$ event illustrated in this figure contains 10 energy depositions. The scoring sphere is placed at a random distance which is less or equal to the domain radius (light blue circle). It is in a random direction from a randomly selected energy deposition (red circle). In this illustration, the lineal energy is obtained by summing the three energy depositions contained in the domain sphere, and its associated statistical weight is taken as 10/3.

Table 2. An example of calculation method for frequency mean lineal energy from Geant4 simulation. Among the parameters in the Table, y range is an example to show how to draw the lineal energy frequency graph. Lineal energy for i -th event belongs to the $(k-1)$ -th bin of lineal energy histogram.

Event number	Lineal energy (y)	y range	Weight (w)
1	y_1	Δy_{k-1}	w_1
2	y_2	Δy_k	w_2
3	y_3	Δy_{k+1}	w_3
4	y_4	Δy_{k+1}	w_4
5	y_5	Δy_k	w_5
\vdots	\vdots	\vdots	\vdots
$i - 1$	y_{i-1}	Δy_k	w_{i-1}
i	y_i	Δy_{k-1}	w_i
\vdots	\vdots	\vdots	\vdots
n	y_n	Δy_k	w_n

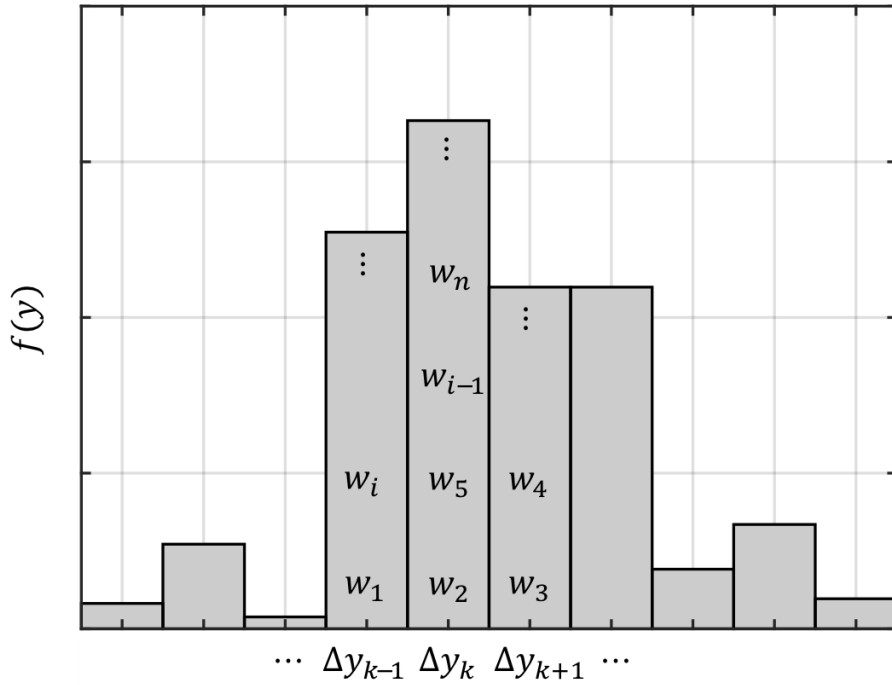


Figure 5. An example of lineal energy frequency, $f(\mathbf{y})$ corresponding to **Table 2**. Weighting w_i is added according to which range the lineal energy generated in the i -th event belongs. Finally, $f(\mathbf{y})$ is the summation of all weightings in each bin.

The \bar{y}_D simulations with real cell images were split into three steps as shown in **Figure 6**. The spectra of a 150 kVp polychromatic x-ray beam with a 2 mm aluminum filter were obtained using SpekCalc 1.1 [36]. The phase space file (phsp1) was recorded for 150 kVp x-ray photon beam passing a 1.9 cm diameter area at 1 mm depth in a macroscopic water phantom (**Figure 6. (a)**). Then it was used to irradiate a single GNP (**Figure 6. (b)**). Note that each particle was weighted by $1/\cos(\theta)$ based on the angle (θ) between its original direction and the beam axis to account for contributions of laterally scattered electrons. The phase space file (phsp2) was recorded on the GNP surface to score outgoing electrons. This file was used as a source at each center of GNPs in the cell-sized water phantom (**Figure 6. (c)**). For the fourth step, the probability density function of lineal energy ($f(y)$) was obtained from the scores of all energy depositions occurring in the domain volume (**Figure 6. (d)**). The default domain radius (r_d) was set to be 500 nm.

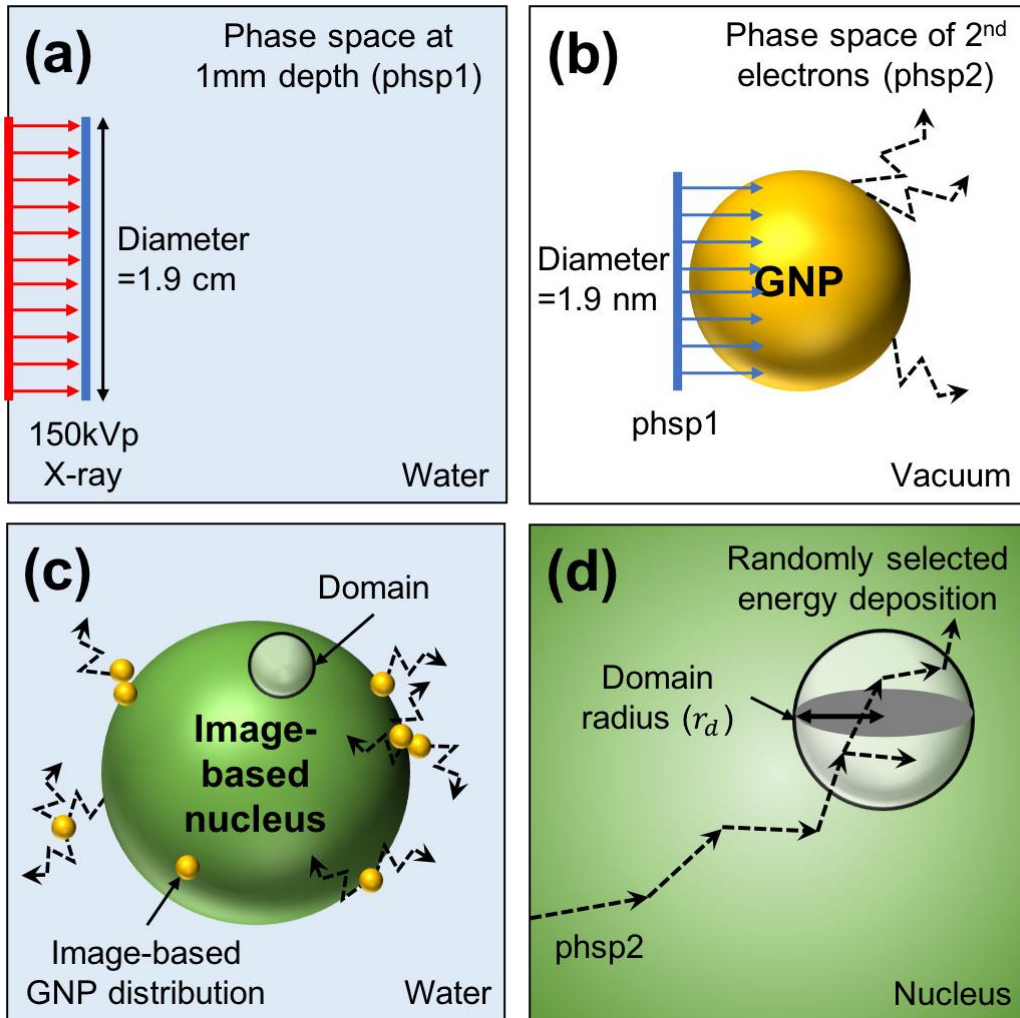


Figure 6. Schematic diagram for \bar{y}_D simulation geometry (not to scale) (a) The phase space file (phsp1) was recorded for 150 kVp x-ray photon beam passing a 1.9 cm diameter area at 1 mm depth in a macroscopic water phantom. (b) A 1.9 nm GNP was irradiated by the phsp1 in vacuum. The outgoing electrons were scored in a phase space file (phsp2) on the surface of GNP. (c) The phase space was used as a point source at each center of GNPs of which positions were based on ODT images. (d) The domain volume is randomly placed within the nucleus and one energy deposition was sampled to produce lineal energy (y).

2.G. Comparison of GNP-LEM and GNP-MKM

The radio-enhancement has been often expressed in terms of sensitizer enhancement ratio (SER) [4, 12-14]. SER was calculated from the mean inactivation dose (MID), defined as the area under the survival fraction curve [39]. It is a useful concept for specifying intrinsic radio-sensitivity of biological cell systems and is endorsed by ICRU report 30 [39]. The MID for gold-treated cells was obtained from the dose response curve calculated by GNP-MKM and GNP-LEM.

$$MID = \int_0^{\infty} S(D)dD \quad (14)$$

$$SER = \frac{MID_{w/o.GNP}}{MID_{GNP}} \quad (15)$$

At the same time, the increase in killing was presented to as the relative biological effectiveness (RBE), which is defined by a dose ratio at same endpoint (10%).

In order to evaluate the sensitivity of the parameters used in two models, percentages of SER change with $\pm 25\%$ and $\pm 50\%$ of D_t ($=20$ Gy) and r_d ($=500$ nm) were calculated. According to Sung et al. [13], SER is 1.34 in case of MDA-MB-231 cells exposed to 150 kVp x-rays after 500 $\mu\text{g/ml}$ GNPs treatment. In addition, the best-fit value of r_d to this experimental result was determined by minimizing the root mean square error (RMSE) among various r_d ($= 1$ nm~10 μm) with 5 nm bin intervals.

3. Results

3.A. Common variables in both models

The lineal quadratic equation parameters, $\alpha = 0.02 \text{ [Gy}^{-1}]$ and $\beta = 0.058 \text{ [Gy}^{-2}]$ were obtained for MDA-MB-231 irradiated with 150 kVp. The number of GNPs in a cell was set to be $3.40 \pm 0.04 \times 10^7$ [13], which was determined by inductively coupled plasma-mass spectrometry (ICP-MS). It was calculated from the total mass of gold per cells treated with 1.9 nm GNPs (Nanoprobes Inc. Yaphank, NY) of 500 $\mu\text{g/ml}$.

The interaction probability of GNP irradiated by 150 kVp was calculated to be 4.4×10^{-6} interactions per Gy per GNP. **Table 3** shows the interaction probability of GNPs and WNP per Gy at 1 mm depth between a 1.9nm GNP and various photon sources. The ratios of GNP and WNP for each beam were 1.4, 1.0, and 1.0, respectively.

Table 3. The interaction probability per Gy at 1 mm depth between 1.9nm single GNP and different photon sources

Interaction probability [/Gy]		Photon sources		
		150 kVp	6 MV (PDD100)	¹⁹² Ir
GNP	Produced by photons	1.7×10^{-6}	3.8×10^{-9}	6.6×10^{-8}
	Produced by electrons	2.8×10^{-6}	4.5×10^{-5}	1.7×10^{-5}
	Total	4.4×10^{-6}	4.5×10^{-5}	1.7×10^{-5}
WNP	Produced by photons	8.8×10^{-9}	1.8×10^{-10}	1.3×10^{-9}
	Produced by electrons	3.2×10^{-6}	4.5×10^{-5}	1.7×10^{-5}
	Total	3.2×10^{-6}	4.5×10^{-5}	1.7×10^{-5}
Ratio of GNP and WNP		1.4	1.0	1.0

3.B. MC simulation of \bar{y}_D

To validate the calculation method of \bar{y}_D , **Figure 7** was reproduced with the same simulation condition from Kyriakou et al [32]. The Geant4-DNA low-energy extension of Geant4 includes sets of physics models that enable track-structure (i.e., step-by-step) simulation of charged particle transport in liquid water down to the eV energy range. Regarding the simulation of electron interaction, three physics models were used: the default Geant4-DNA models (“option2”) [34], the models developed at the University of Ioannina (“option4”) [40, 41], and the CPA100 models [42]. Using these models, frequency-mean lineal energy and dose-mean lineal energy were calculated with different incident electron kinetic energies (**Figure 7**).

Depending on the domain sizes, the \bar{y}_D had a range from 1 keV/ μm to 20.4 keV/ μm . **Table 4** shows the results of calculating the dose-mean lineal energy for a simple cellular geometry and GNP uptake as described in **Figure 2**. (a) and (b). The domain radius is the average radius of a series of spheres created by transforming each domain in the nucleus into an equal unit density area [21]. The biological meaning corresponding to each domain size [32, 43] are listed in **Table 4**. Frequency weighted lineal energy spectra and dose weighted lineal energy spectra with 500nm domain radius of cells with GNP was similar to that of cells without GNP (**Figure 8**).

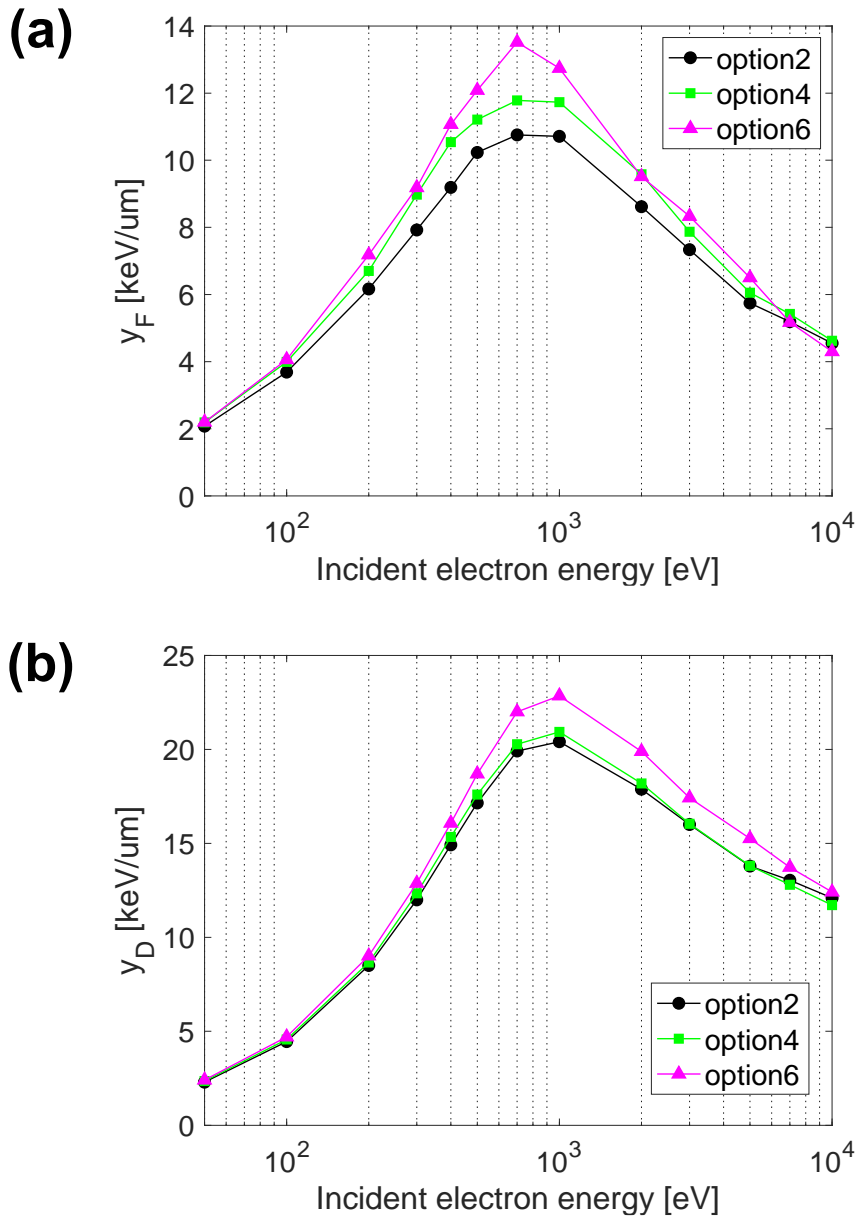


Figure 7. Validation of microdosimetric spectra (a) Frequency-mean lineal energy and (b) dose-mean lineal energy as a function of incident electron kinetic energy, in scoring spheres of 500 nm radius; Black circles: “option 2” constructor (default models); green squares: “option 4” constructor (Ioannina models); pink triangles: “option 6” constructor (CPA100 models); Reproduced from [32] for validation.

Table 4. Dose-mean lineal energy, \bar{y}_D with different domain sizes, r_d of secondary radiations from GNP incident with 150 kVp x-ray

r_d	1 nm	5 nm	15 nm	150 nm
Biological meaning	Base pair	Nucleosome	Chromatin	Chromosome
\bar{y}_F [keV/ μm]	5.32	5.99	4.25	2.39
\bar{y}_D [keV/ μm]	20.43	16.25	13.13	6.42
r_d	300 nm	500 nm	4 μm	10 μm
Biological meaning	Liposome	Metaphase chromosome	Nucleus	Cell
\bar{y}_F [keV/ μm]	2.17	1.92	0.84	0.33
\bar{y}_D [keV/ μm]	5.24	4.47	1.63	0.98

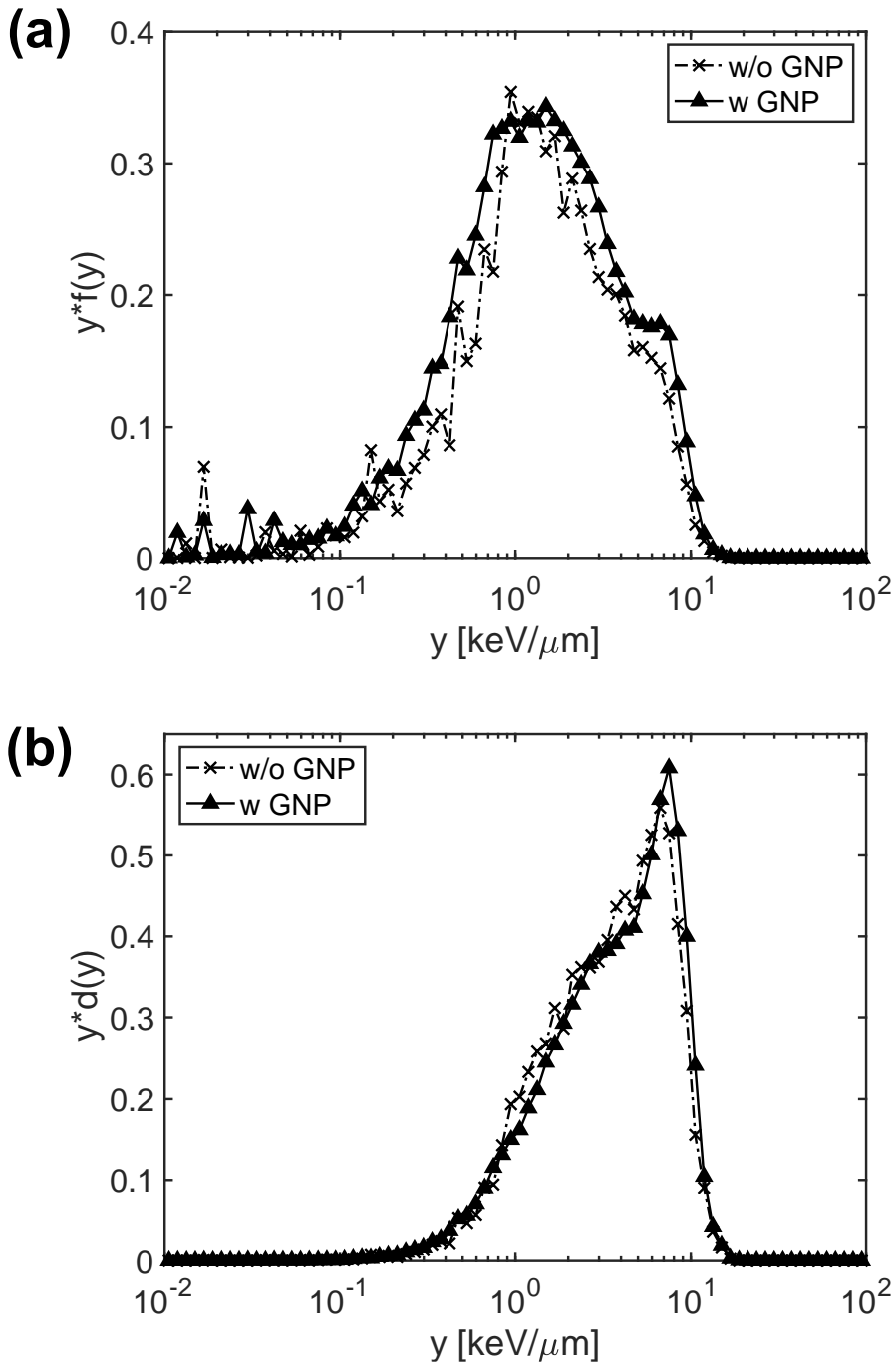


Figure 8. (a) Frequency weighted lineal energy spectra (b) dose weighted lineal energy spectra of 500 nm domain radius; the bin width of the x-axis is set as 0.05.

3.C. Cellular geometry and GNP distributions

Figure 9 (a) and (b) are examples of cell nucleus structure and gold nanoparticle distribution obtained by reprocessing the ODT image. **Figure 10** is an average refractive index values for various regions in a cell which is treated by 1.9 nm GNPs of 500 $\mu\text{m}/\text{ml}$ for 24 hours. **figure 11** shows integrated gold signal of ODT images from 5 cells for increasing distance from the nuclear membrane. The gold intensity reduces significantly across the membrane (distance = 0) and the gold signal within the nucleus (distance < 0) is consistent with the assumption that all of the gold is nearly outside the nuclear membrane.

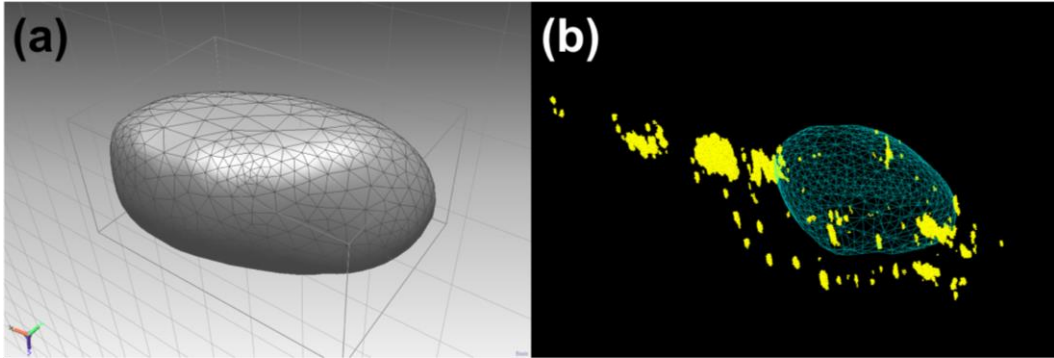


Figure 9. Cell nucleus reconstructed from ODT images: (a) Cell nucleus polygon displayed in 3D program (b) Image-based cell nucleus and GNP distributions imported to the Geant4 simulation tool

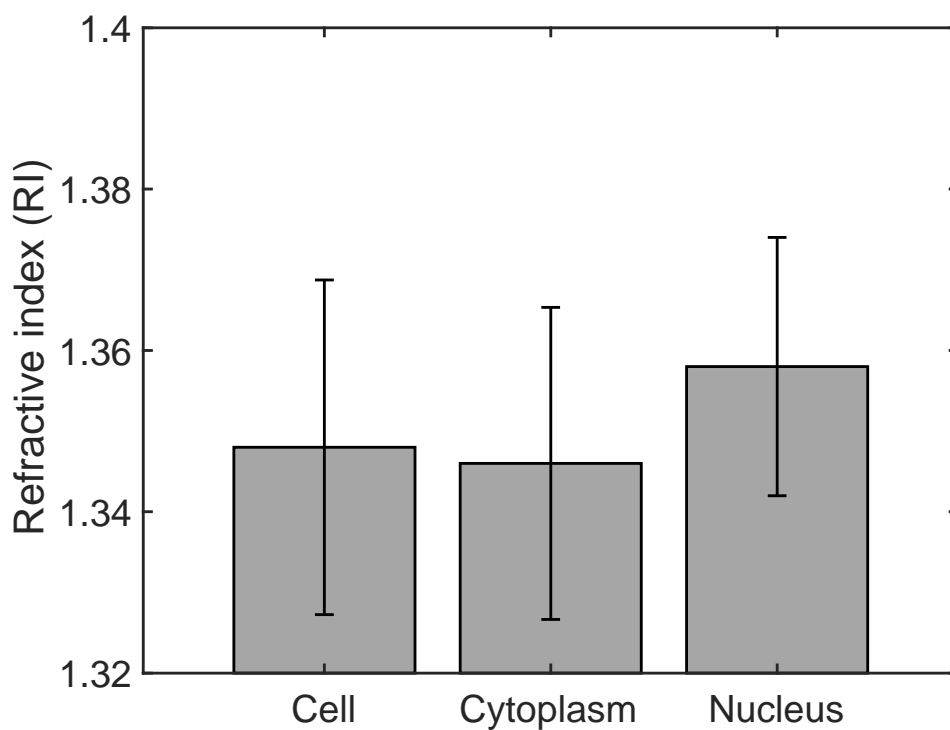


Figure 10. Average refractive index values for various regions in a cell which is treated by 1.9 nm GNPs of 500 $\mu\text{m}/\text{ml}$ for 24 hours.

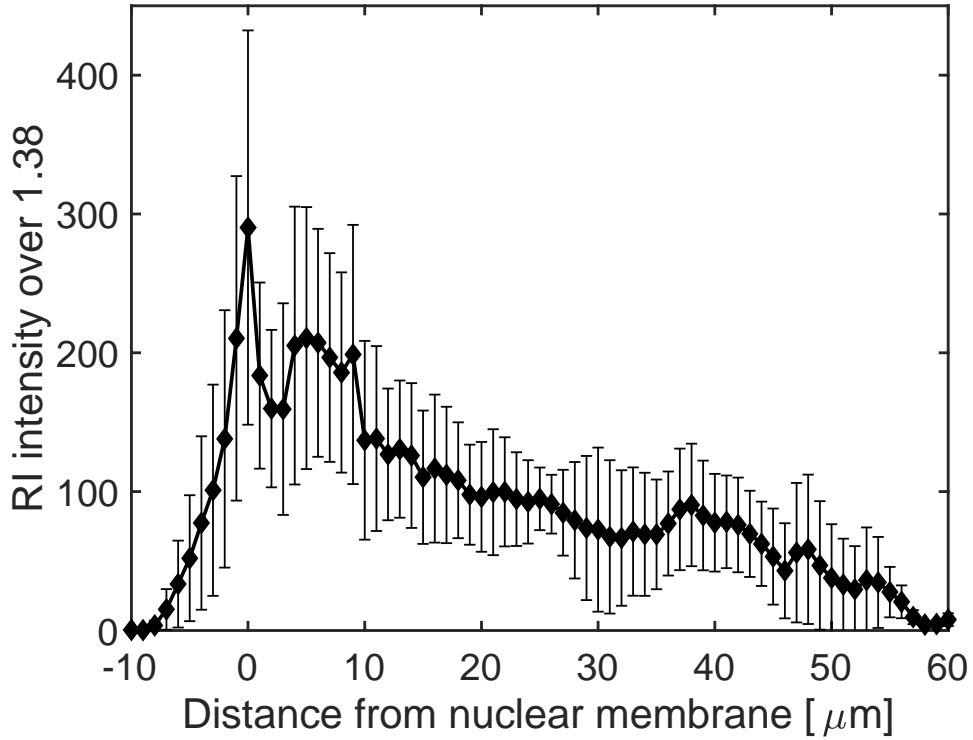


Figure 11. Integrated gold signal of ODT images from 5 cells for increasing distance from the nuclear membrane. The gold intensity reduces significantly across the membrane (distance = 0) and the gold signal within the nucleus (distance < 0) is consistent with the assumption that all of the gold is nearly outside the nuclear membrane.

3.D. Comparison of GNP-MKM and GNP-LEM

The results of GNP-MKM with different GNP concentrations are summarized in **Table 5**. The dose-mean lineal energy of 2nd radiations from the GNPs (=4.47 keV/ μm) showed slightly higher than that of the photon beam (=4.24 keV/ μm). Cellular GNP distributions were obtained from 3D images of five cells observed by the ODT method. The GNP distributions were obtained from the 3D ODT images of five cells. They were combined with GNP-MKM to predict cell survival as shown in **Table 6**.

The error bars for GNP-LEM and GNP-MKM indicated the variation due to differences in cellular GNP distributions in **Figure 12**. **Figure 13** shows SER changes to adjustable parameters with $\pm 25\%$ and $\pm 50\%$ of D_t (=20 Gy) and r_d (=500 nm). The SERs predicted by GNP-MKM and GNP-LEM were 1.32~2.13 and 1.29, respectively. Their dependencies of SER results indicated that GNP-MKM predictions were more sensitive than the GNP-LEM results with respect to D_t selection for relative fluctuations in r_d .

Table 5. Comparison of GNP-MKM MKM ($r_d = 500 \text{ nm}$) and GNP-LEM ($D_t = 20 \text{ Gy}$) by using a simple cell geometry irradiated by 150 kVp x-ray with different GNP concentrations

$(r_d = 500 \text{ nm},$ $D_t = 20 \text{ Gy})$	Number of GNPs [/cell]				
	w/o GNP	1×10^6	5×10^6	1×10^7	5×10^7
$\bar{y}_D \text{ [keV}/\mu\text{m}]$	4.24	4.47	4.47	4.47	4.47
$D_n \text{ [Gy]}$	1	1.03	1.14	1.28	2.40
SER (GNP-MKM)	-	1.15	1.28	1.45	2.82
SER (GNP-LEM)	-	1.03	1.15	1.29	2.54
RBE (D_{10}) (GNP-MKM)	-	1.11	1.22	1.39	2.54
RBE (D_{10}) (GNP-LEM)	-	1.03	1.15	1.30	2.44

Table 6. Comparison of GNP-MKM MKM ($r_d = 500 \text{ nm}$) and GNP-LEM ($D_t = 20 \text{ Gy}$) by using real cell geometry obtained from five ODT images irradiated by 150 kVp x-ray with 500 $\mu\text{m}/\text{ml}$ GNPs

$(r_d = 500 \text{ nm},$ $D_t = 20 \text{ Gy})$	ODT images					
	Cell1	Cell2	Cell3	Cell4	Cell5	Avg.
$\bar{y}_D \text{ [keV}/\mu\text{m}]$	4.47	4.47	4.47	4.47	4.47	4.47
$D_n \text{ [Gy]}$	1.48	1.12	1.62	1.08	1.12	1.28
SER (GNP-MKM)	1.68	1.26	1.85	1.21	1.26	1.41
SER (GNP-LEM)	1.50	1.14	1.81	1.09	1.15	1.29
RBE (D_{10}) (GNP-MKM)	1.61	1.20	1.74	1.15	1.20	1.33
RBE (D_{10}) (GNP-LEM)	1.49	1.13	1.79	1.09	1.15	1.24

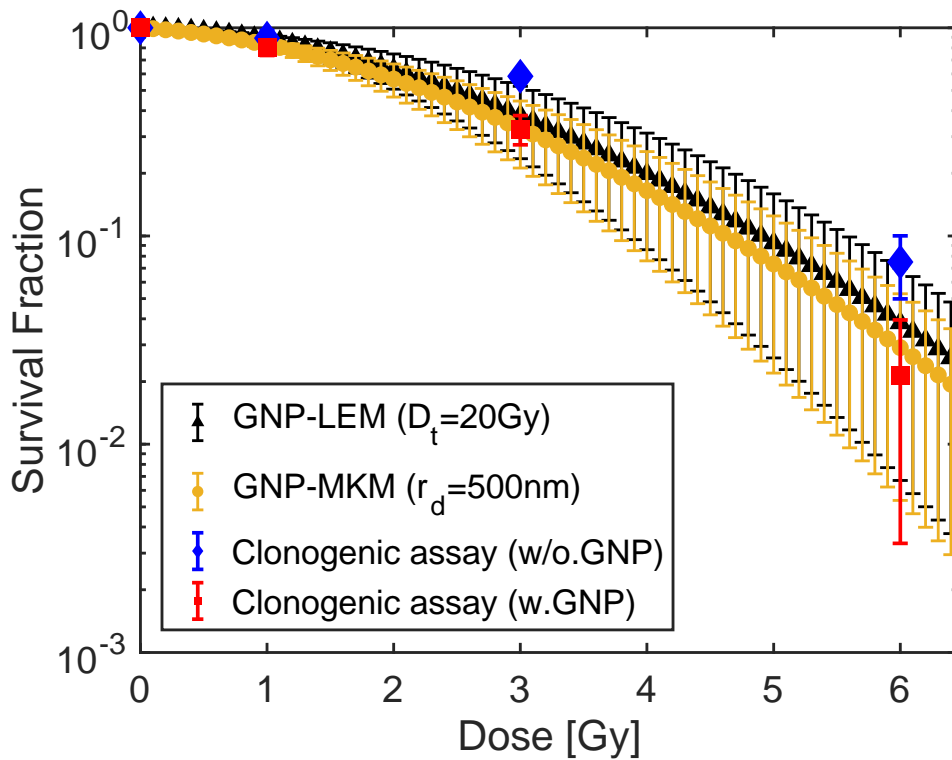


Figure 12. Experimentally observed cell survival for MDA-MB-231 cells exposed to 1, 3, and 6 Gy of 150 kVp x-rays (red square = with GNP; blue diamond = without GNP) and theoretically predicted survival fraction with GNPs (black triangle by LEM; yellow circle by MKM). Error bars are one standard deviation at each corresponding dose-survival fraction point.

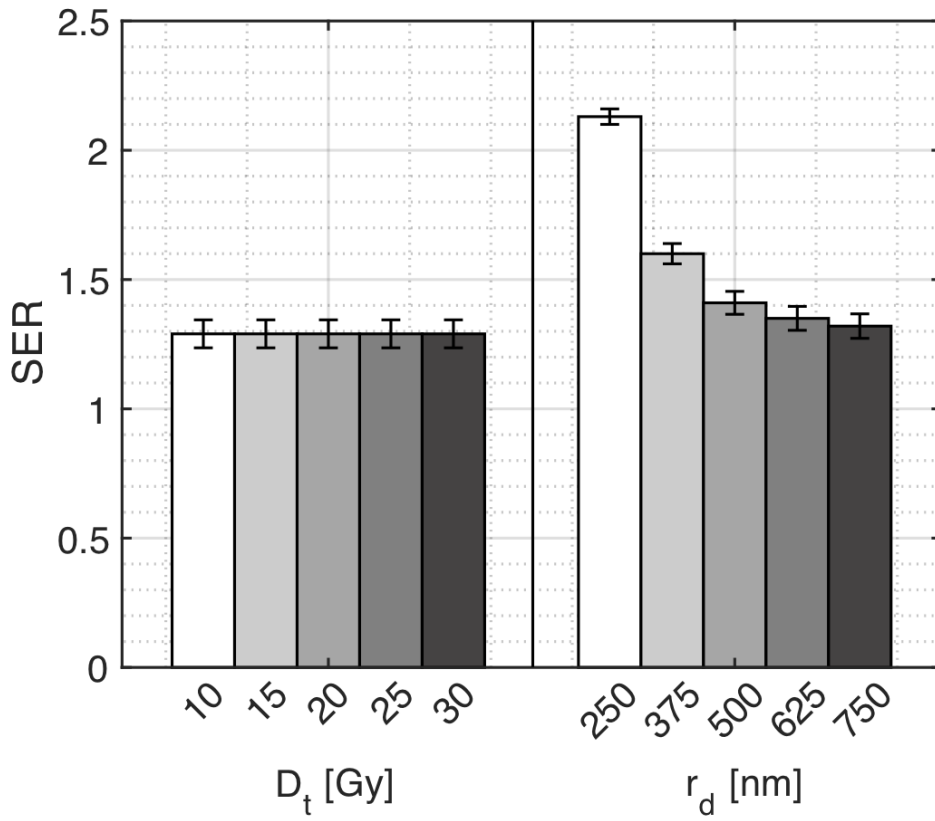


Figure 13. SER sensitivity of adjustable parameters in the models expressed as a percentage of SER changes with $\pm 25\%$ and $\pm 50\%$ of D_t ($=20$ Gy) and r_d ($=500$ nm).

4. Discussion

Depending on the domain sizes, the \bar{y}_D had a range from 0.98 keV/ μm to 20.4 keV/ μm (**Table 4**). A higher \bar{y}_D was observed when the range of electrons corresponded to the domain size, which indicated a strong dependency between \bar{y}_D and domain size. The maximum lineal energies of electrons can be calculated based on continuous slowing down approximation (CSDA) range and stopping power data [44]. For example, a 5.8 keV electron deposits its entire energy in 1 μm domain volume, where electron range equals the site diameter. After dividing it by mean chord length, maximum lineal energy of 8.7 keV/ μm was obtained. For this reason, the choice of domain radius is important in determining the relative biological effectiveness (RBE).

The domain size is related to biological effects. The lethal lesions are produced by not only simple chromosome breaks with nanometer domains but also a pairwise combination of DSBs with micrometers domain sizes [17]. In addition, Matsuya Y. [45] has shown that there is a proportional relationship between dose mean lineal energy and DSB with a 500 nm domain radius (1 μm diameter). It varies for each experiment to best-fit between the MKM and clonogenic assays [46]. It has been found that when fitting the different proton RBE data, r_d value is 282 nm for human salivary gland cells [47]. In this study, r_d was decided between 490 nm and 495 nm for MDA-MB-231 cells to estimate RBE for GNP radiotherapy in this study. It had the least RMSE of 0.01 with a measured cell survival curve. This domain size ($=2r_d$), which is almost 1 μm , represented a pairwise combination of DSBs, which makes it hard to repair the DNA damage. It contributes to the idea that the DNA repair mechanisms have been modified, supporting recent studies [48] that mention the biological effect of the intracellular GNPs as radiosensitizers in addition to radio-enhancers.

According to **Table 5**, dose-mean linear energy was independent on GNP concentrations. The simulated \bar{y}_D without GNP ($=4.24$ keV/ μm) in **Table 5** agreed with published data, 4.2 keV/ μm [22]. Even though the frequency of lineal energy is increased

with larger number of GNPs, the dose-mean lineal energy (\bar{y}_D) is the same due to the same radiation characteristics from a single GNP. Chun-Hui Hsing group only applied dose-mean lineal energy (\bar{y}_D) to calculate increased RBE for GNP radio-enhancement [18]. However, according to the results (**Table 5**), the dose-mean lineal energy alone does not account for the effects of GNP concentration, which is opposed to the previous experimental results [49]. Instead, it depends on incident photon energy, which makes different energy range of secondary electrons.

Both models showed good agreement with the experimental in vitro cell survival data based on 3D images of live breast cancer cells and the GNP uptake within the cells (**Figure 12**). The GNP-MKM with 500 nm domain radius and GNP-LEM with 20 Gy threshold dose had RMSE values of 0.014, and 0.052, respectively. However, it was assumed that all image voxels with RI values higher than 1.38 contained the same number of GNPs per voxel (**Figure 3** and **Figure 9**). Since higher RI values indicated a larger number of GNPs, other techniques such as fluorescence imaging are necessary to determine quantitative correlations of RI values and GNP concentration.

In addition, when simulating secondary radiations from GNPs, a GNP surface coating was ignored. The 1.9 nm GNPs (Nanoprobes Inc., Yaphank, NY) used in this study were coated with a layer of thiol, which made their surface thickness about 0.7 nm. However, B Koger et al. [50] showed reductions in dose enhancement due to the inclusion of the GNP surface with a polyethylene glycol (PEG) coatings by using PENELOPE Monte Carlo simulation toolkit. Over the first 500 nm surrounding a single GNP, the presence of a PEG surface coating reduced dose by 5~26 % for 2 nm diameter GNPs for incident photon energies ranging from 1 keV to 200 keV and coating thicknesses of 10 and 20 nm. For more accurate simulation of GNP dose enhancement, the GNP surface coating should be taken into consideration.

The most significant differences between MKM and LEM were adjustable parameters, threshold dose (D_t) and domain size (r_d). Their dependencies of SER results indicated that GNP-MKM predictions were more sensitive than the GNP-LEM results with

respect to D_t selection for relative fluctuations in r_d (**Figure 13**), as presented similarly in Kase et al [19].

The predictions from both modeling can be used to design clinical trials. So far, there has been no clinical study evaluating the GNP radio-enhancement [51]. Gold-based nanomaterials have yet received FDA approval in 2020 [48]. In comparison, several other high-Z nanoparticles are currently undergoing clinical investigation [51]. For example, a Phase I study of gadolinium-based nanoparticles is used for treatment of multiple brain metastases by whole brain RT (AGuIX; NCT02820454, i.v. injection). Hafnium oxide crystalline nanoparticle are under Phase I/II evaluation with SBRT for liver cancer treatment (NBTXR3; NCT02721056, intralesional or super selective transcatheter arterial injection) [52]. It is also being investigated with external beam RT as preoperative treatment for soft tissue sarcoma in Phase II/III studies (NBTXR3; NCT02379845, intra-tumoral injection) [53]. In addition, with brachytherapy or IMRT, it is under Phase I/II investigation for the prostate cancer treatment (NBTXR3; NCT02805894, intra-tumoral injection). Although clinical studies of GNPs as radio-enhancement are currently lacking, GNP-LEM and GNP-MKM can be used to predict the RBE value for applications in future clinical stage.

5. Conclusions

Both GNP-MKM and GNP-LEM have shown good agreement with the experimental in vitro cell survival data based on 3D images of live breast cancer cells and the GNP uptake within the cells. The most significant difference between the MKM and the LEM is related to the definition of the input parameters. As a result of GNP-MKM, the optimized domain size of about 1 μm , represented a pairwise combination of DSBs, which makes it hard to repair the DNA damage. It contributes to the idea that the DNA repair mechanisms have been modified, which make the biological effect of the intracellular GNPs as radiosensitizers in addition to radio-enhancers. GNP-MKM predictions were slightly more sensitive to relative variations of the domain size than the GNP-LEM results concerning the choice of threshold doses. Although this is a specific case study, the GNP-LEM and GNP-MKM provide a useful method to predict survival fraction for the GNP radio-enhancement. The predictions from both modeling can be used to predict the RBE value applied in future clinical stage of GNP-mediated radiotherapy.

REFERENCES

1. Schuemann, J., et al., *Roadmap for metal nanoparticles in radiation therapy: current status, translational challenges, and future directions*. Physics in Medicine & Biology, 2020.
2. Hainfeld, J.F., D.N. Slatkin, and H.M. Smilowitz, *The use of gold nanoparticles to enhance radiotherapy in mice*. Physics in Medicine & Biology, 2004. **49**(18): p. N309.
3. Hainfeld, J.F., et al., *Gold nanoparticles enhance the radiation therapy of a murine squamous cell carcinoma*. Physics in Medicine & Biology, 2010. **55**(11): p. 3045.
4. Jain, S., et al., *Cell-specific radiosensitization by gold nanoparticles at megavoltage radiation energies*. International Journal of Radiation Oncology* Biology* Physics, 2011. **79**(2): p. 531-539.
5. Kunjachan, S., et al., *Nanoparticle mediated tumor vascular disruption: a novel strategy in radiation therapy*. Nano letters, 2015. **15**(11): p. 7488-7496.
6. Rahman, W.N., et al., *Enhancement of radiation effects by gold nanoparticles for superficial radiation therapy*. Nanomedicine: Nanotechnology, Biology and Medicine, 2009. **5**(2): p. 136-142.
7. Lechtman, E., et al., *A Monte Carlo-based model of gold nanoparticle radiosensitization accounting for increased radiobiological effectiveness*. Physics in Medicine & Biology, 2013. **58**(10): p. 3075.
8. Lin, Y., et al., *Comparing gold nano-particle enhanced radiotherapy with protons, megavoltage photons and kilovoltage photons: a Monte Carlo simulation*. Physics in Medicine & Biology, 2014. **59**(24): p. 7675.

9. Lin, Y., et al., *Gold nanoparticle induced vasculature damage in radiotherapy: Comparing protons, megavoltage photons, and kilovoltage photons*. Medical Physics, 2015. **42**(10): p. 5890-5902.
10. McMahon, S.J., et al., *Biological consequences of nanoscale energy deposition near irradiated heavy atom nanoparticles*. Scientific reports, 2011. **1**: p. 18.
11. Sung, W., S. Jung, and S.-J. Ye, *Evaluation of the microscopic dose enhancement for nanoparticle-enhanced Auger therapy*. Physics in Medicine & Biology, 2016. **61**(21): p. 7522.
12. Lin, Y., et al., *Biological modeling of gold nanoparticle enhanced radiotherapy for proton therapy*. Physics in Medicine & Biology, 2015. **60**(10): p. 4149.
13. Sung, W., et al., *Computational modeling and clonogenic assay for radioenhancement of gold nanoparticles using 3D live cell images*. Radiation research, 2018. **190**(5): p. 558-564.
14. Sung, W., et al., *Dependence of gold nanoparticle radiosensitization on cell geometry*. Nanoscale, 2017. **9**(18): p. 5843-5853.
15. Elsässer, T. and M. Scholz, *Cluster effects within the local effect model*. Radiation research, 2007. **167**(3): p. 319-329.
16. ICRU, M., *Report 36*. International Commission on Radiation Units and Measurements, Bethesda, MD, 1983.
17. Santa Cruz, G.A., *Microdosimetry: Principles and applications*. Reports of Practical Oncology & Radiotherapy, 2016. **21**(2): p. 135-139.
18. Hsing, C.-H., et al., *GNP enhanced responses in microdosimetric spectra for ¹⁹²Ir source*. Radiation Measurements, 2018. **118**: p. 67-71.
19. Kase, Y., et al., *Biophysical calculation of cell survival probabilities using*

- amorphous track structure models for heavy-ion irradiation*. Physics in Medicine & Biology, 2007. **53**(1): p. 37.
20. Hawkins, R.B., *A statistical theory of cell killing by radiation of varying linear energy transfer*: Radiation research, 1994. **140**(3): p. 366-374.
 21. Hawkins, R.B., *A microdosimetric-kinetic model for the effect of non-Poisson distribution of lethal lesions on the variation of RBE with LET*. Radiation research, 2003. **160**(1): p. 61-69.
 22. Kase, Y., et al., *Microdosimetric measurements and estimation of human cell survival for heavy-ion beams*. Radiation research, 2006. **166**(4): p. 629-638.
 23. Kase, Y., et al., *Microdosimetric approach to NIRS-defined biological dose measurement for carbon-ion treatment beam*. Journal of radiation research, 2011. **52**(1): p. 59-68.
 24. Rafehi, H., et al., *Clonogenic assay: adherent cells*. JoVE (Journal of Visualized Experiments), 2011(49): p. e2573.
 25. Coulter, J.A., et al., *Cell type-dependent uptake, localization, and cytotoxicity of 1.9 nm gold nanoparticles*. International journal of nanomedicine, 2012. **7**: p. 2673.
 26. McMahon, S.J., et al., *Nanodosimetric effects of gold nanoparticles in megavoltage radiation therapy*. Radiotherapy and Oncology, 2011. **100**(3): p. 412-416.
 27. McQuaid, H.N., et al., *Imaging and radiation effects of gold nanoparticles in tumour cells*. Scientific reports, 2016. **6**: p. 19442.
 28. Kim, D., et al., *Label-free high-resolution 3-D imaging of gold nanoparticles inside live cells using optical diffraction tomography*. Methods, 2018. **136**: p. 160-167.
 29. Lee, J., et al., *Deep-learning-based label-free segmentation of cell nuclei in time-lapse refractive index tomograms*. IEEE Access, 2019. **7**: p. 83449-83460.

30. Agostinelli, S., et al., *GEANT4—a simulation toolkit*. Nuclear instruments and methods in physics research section A: Accelerators, Spectrometers, Detectors and Associated Equipment, 2003. **506**(3): p. 250-303.
31. Allison, J., et al., *Geant4 developments and applications*. IEEE Transactions on nuclear science, 2006. **53**(1): p. 270-278.
32. Kyriakou, I., et al., *Microdosimetry of electrons in liquid water using the low-energy models of Geant4*. Journal of Applied Physics, 2017. **122**(2): p. 024303.
33. Bernal, M., et al., *Track structure modeling in liquid water: A review of the Geant4-DNA very low energy extension of the Geant4 Monte Carlo simulation toolkit*. Physica Medica, 2015. **31**(8): p. 861-874.
34. Incerti, S., et al., *The geant4-dna project*. International Journal of Modeling, Simulation, and Scientific Computing, 2010. **1**(02): p. 157-178.
35. Incerti, S., et al., *Comparison of GEANT4 very low energy cross section models with experimental data in water*. Medical physics, 2010. **37**(9): p. 4692-4708.
36. Poludniowski, G., et al., *SpekCalc: a program to calculate photon spectra from tungsten anode x-ray tubes*. Physics in Medicine & Biology, 2009. **54**(19): p. N433.
37. Tillikainen, L., et al., *Determination of parameters for a multiple-source model of megavoltage photon beams using optimization methods*. Physics in Medicine & Biology, 2007. **52**(5): p. 1441.
38. Ye, S.J., E.I. Parsai, and J.J. Feldmeier, *Dosimetric characteristics of a linear array of γ or β -emitting seeds in intravascular irradiation: Monte Carlo studies for the AAPM TG-43/60 formalism*. Medical Physics, 2003. **30**(3): p. 403-414.
39. Subiel, A., R. Ashmore, and G. Schettino, *Standards and methodologies for characterizing radiobiological impact of high-Z nanoparticles*. Theranostics, 2016. **6**(10): p. 1651.

40. Kyriakou, I., S. Incerti, and Z. Francis, *Improvements in geant4 energy-loss model and the effect on low-energy electron transport in liquid water*. Medical physics, 2015. **42**(7): p. 3870-3876.
41. Kyriakou, I., et al., *The impact of new Geant4-DNA cross section models on electron track structure simulations in liquid water*. Journal of Applied Physics, 2016. **119**(19): p. 194902.
42. Bordage, M., et al., *Implementation of new physics models for low energy electrons in liquid water in Geant4-DNA*. Physica Medica, 2016. **32**(12): p. 1833-1840.
43. Schubert, I. and J. Oud, *There is an upper limit of chromosome size for normal development of an organism*. Cell, 1997. **88**(4): p. 515-520.
44. Berger, M.J., *ESTAR, PSTAR, and ASTAR: Computer programs for calculating stopping-power and range tables for electrons, protons, and helium ions*. esta, 1992.
45. Matsuya, Y., et al., *Quantitative estimation of DNA damage by photon irradiation based on the microdosimetric-kinetic model*. Journal of Radiation Research, 2014. **55**(3): p. 484-493.
46. Newpower, M., et al., *Using the proton energy spectrum and microdosimetry to model proton relative biological effectiveness*. International Journal of Radiation Oncology* Biology* Physics, 2019. **104**(2): p. 316-324.
47. Takada, K., et al., *Validation of the physical and RBE-weighted dose estimator based on PHITS coupled with a microdosimetric kinetic model for proton therapy*. Journal of radiation research, 2018. **59**(1): p. 91-99.
48. Penninckx, S., et al., *Gold Nanoparticles as a Potent Radiosensitizer: A Transdisciplinary Approach from Physics to Patient*. Cancers, 2020. **12**(8): p. 2021.
49. Rosa, S., et al., *Biological mechanisms of gold nanoparticle radiosensitization*. Cancer nanotechnology, 2017. **8**(1): p. 2.

50. Koger, B. and C. Kirkby, *Dosimetric effects of polyethylene glycol surface coatings on gold nanoparticle radiosensitization*. *Physics in Medicine & Biology*, 2017. **62**(21): p. 8455.
51. Cui, L., et al., *Radiosensitization by gold nanoparticles: Will they ever make it to the clinic?* *Radiotherapy and Oncology*, 2017. **124**(3): p. 344-356.
52. Bonvalot, S., et al., *First-in-human study testing a new radioenhancer using nanoparticles (NBTXR3) activated by radiation therapy in patients with locally advanced soft tissue sarcomas*. *Clinical Cancer Research*, 2017. **23**(4): p. 908-917.
53. Bonvalot, S., et al., *NBTXR3, a first-in-class radioenhancer hafnium oxide nanoparticle, plus radiotherapy versus radiotherapy alone in patients with locally advanced soft-tissue sarcoma (Act. In. Sarc): A multicentre, phase 2–3, randomised, controlled trial*. *The Lancet Oncology*, 2019. **20**(8): p. 1148-1159.

Abstract (in Korean)

국 문 초 록

방사선 증감제로서의 금나노입자 효과는 수많은 선행연구에서 이미 검증된 바이다. 금나노입자 증감 효과에 의한 암세포의 생존율을 예측하기 위하여 로컬 이펙트 모델(Local Effective Model; LEM)이 도입되었으며, 500 $\mu\text{g/ml}$ 농도의 금나노입자를 섭취시킨 뒤 150 kVp 방사선 조사를 한 MDA-MB-231 유방암 세포의 생존율을 성공적으로 예측하였다. 하지만 세포 안에서 일어나는 생물학적 영향과 관련된 측정 가능한 미시선량계측 인자(microdosimetric quantities)를 얻을 수 없는 한계점이 있었다. 따라서 본 연구에서는 평균 선형에너지 선량(dose-mean lineal energy)과 같은 미시선량계측 인자를 사용하는 마이크로-키네틱 모델(Microdosimetric-Kinetic Model; MKM)을 도입하여 금나노입자의 증감 효과를 예측하고자 하였다. 몬테카를로 시뮬레이션 툴킷 중 하나인 Geant4를 사용하여 금나노입자로부터 방출되는 2차 방사선의 평균 선형에너지 선량과 금나노입자 주변의 방사형 선형 분포를 추정하였다. 또한 기존의 로컬 이펙트 모델과 비교하기 위하여 서로 다른 도메인 크기, 금나노입자의 농도 등에 대해 각 모델에 사용되는 변수가 어떻게 변화하는지 계산하였다. 마이크로-키네틱 모델을 바탕으로 계산된 500 nm의 도메인 크기는 생물학적으로 DNA 손상 복구가 어려운 양가닥 절단(Double Strand Break; DSB)이 주된 대상임을 의미한다. 이것은 금나노입자가 세포 내에서 DNA 복구 메커니즘을 변형시켜 방사선 증감제 뿐만 아니라 감작제로서 역할을 한다는 선행 연구를 뒷받침 한다. 도메인 반지름을 500 nm로, 문턱 선량을 20 Gy로 설정 하였을 때, 마이크로-키네틱 모델과 로컬 이펙트 모델에 의해 예측된 감수증감비(Sensitizer Enhancement Ratio; SER)는 각각 1.41과 1.29이었다. 마이크로-키네틱 모델이 도메인 크기에 대해 강한 의존성을 보이는 반면, 로컬 이펙트 모델은 문턱 선량에 대해 낮은

민감도를 보였다. 본 연구를 통해 마이크로-키네틱 모델이 금나노입자 증감 효과에 의한 생존율 곡선을 예측하는 또 다른 방법론을 제시할 수 있다는 것을 확인하였다.

주요어: 금나노입자, 방사선 증감 효과, 마이크로-키네틱 모델, 로컬 이펙트 모델, 생존율 곡선, 몬테카를로 시뮬레이션

학 번 : 2017-27243